Intense Femtosecond Pulse Propagation with Applications

J.V. Moloney

Arizona Center for Mathematical Sciences
Department of Mathematics
and
Optical Sciences Center
University of Arizona, Tucson 85721

ABSTRACT

The fundamental physics of high-field laser-matter interactions has driven ultrashort pulse generation to achieve record power densities of 10^{22} Watts per cm^2 in focal spot sizes (FWHM) of 0.8 μm[1]. These enormous fields are generated by compressing longer, high energy pulses to ever shorter lengths using so-called CPA compressors. Great care has to be taken to achieve such record power densities by controlling the spatio-temporal shape during pulse compression. Despite these remarkable experimental achievements, there have been relatively few developments on the theoretical side to derive realistic physical optical material models coupled to sophisticated E.M propagators. Many of the theoretical analysis tools developed in this emerging field of extreme nonlinear optics are restricted to oversimplified 1D models that completely ignore the complex vector spatio-temporal couplings occurring within such small nonlinear interaction volumes.

The advent of these high power ultra-short pulsed laser systems has opened up a whole new vista of applications and computational challenges. The applications space spans relatively short propagation lengths of centimeters to meters to a target up to many kilometers in atmospheric propagation studies. The high local field intensities generated within the pulse can potentially lead to electromagnetic carrier wave shocking so it becomes necessary to fully resolve the optical carrier wave within the 3D propagating pulse envelope. High local field intensities also lead to an explosive growth of the white-light supercontinuum spectrum and the intensities of even remote spectral components can be high enough to generate nonlinear coupling to the host material. For this reason, spectrally local models of light-matter coupling are expected to fail.

In this paper, we will present a fully carrier-resolved E.M. propagator that allows for few meter long propagation lengths while fully resolving the optical carrier wave. Our applications focus will be on the relatively low intensity regime where critical self-focusing collapse in air or water can lead to very strong non-paraxial ultra-broadband excitations. One reason for this restriction is that we do not yet have computationally feasible robust physical models for ultra-broadband excitation of materials where nonlinear dispersion and absorption become dominant. The propagation of terawatt femtosecond duration pulses in the atmosphere can be qualitatively captured by physical models that include reliable linear dispersion/absorption while treating the nonlinear terms as spectrally local. We will review some recent experimental results by the German-Franco Teramobile team on atmospheric propagation, penetration through obscurants and remote laser induced breakdown spectroscopy. As a second application example will address the issue of strongly non-paraxial spectral superbroadening of femtosecond pulses while propagating in water – these latter nonlinear interactions generate so-called nonlinear X- and O-waves depending on the optical carrier wavelength of the initial pulse.

Keywords: Maxwell's equations, ultrashort pulses, critical self-focusing, plasma generation, white light

1. INTRODUCTION

Any investigation of intense ultra-short pulse propagation in nonlinear materials such as air or condensed matter will need to account for strong nonlinear-induced spatial distortion of the pulse as well as severe temporal compression. For example, when multi-terawatt pulses propagate in air, they tend to spontaneously break-up into a chaotic sea of strongly focused light filaments (light strings) embedded in a broad nonlinear pulse background. Each self-focusing filament compresses violently

High-Power Laser Ablation VI, edited by Claude R. Phipps, Proc. of SPIE
Vol. 6261, 626102, (2006) · 0277-786X/06/$15 · doi: 10.1117/12.674881

in space and time until intensities in the nonlinear focal spot reach the optical breakdown threshold. At the same time, the broad pulse background containing the filaments remains relatively flat. The end result is a large spatial scale separation that needs to be resolved. A dilute plasma generated at the peak intensity (10^{13} – 10^{14} Watts per cm^2 in air) creates a negative lens that counteracts the strong positive self-focusing lens and acts to return most of the energy to the broad background pedestal. Relatively little energy is dissipated per self-focusing event (light string creation) thereby making the energy returned to the background available for further light string generation. In this way, a highly dynamic nonlinear waveguide tends to persist over anomalously large distances. Accompanying light string creation is white-light supercontinuum (SC) generation, dilute plasma channel creation and subsequent THz emission from the plasma channel. Within a single multi-terawatt 100 fs pulse, one expects hundreds of such light string creation events at a point in space – moreover the onset of light string generation can be controlled by pre-chirping the laser pulse. The Franco-German Teramobile group has taken the lead in the experimental investigation of fs TW pulse propagation in the atmosphere. An extensive publication list of experiments of this group can be found at the website http://pclasim47.univ-lyon1.fr/publis.html.

We present a physically self-consistent and robust 3D ultrashort pulse propagator that resolves the underlying optical carrier wave while enabling propagation over many meter propagation lengths. Our goal is to retain the full rigor of Maxwell's equations while reducing the problem complexity by constraining the model to unidirectional propagation. As our immediate interest is in very short intense pulse propagation with potentially large induced nonlinear polarization, we will need to accurately capture the very broad spectral landscape that the pulse experiences during its interaction with a host dielectric material. In many cases, spectral superbroadening is such that the generated bandwidth far exceeds in magnitude the underlying carrier frequency $\Delta\omega/\omega << 1$. In this limit, we expect the classical Nonlinear Schrödinger Equation (NLS) propagator to fail. Many attempts have been made to derive nonlinear envelope models that go beyond NLS and we will discuss some of these below when we show explicitly how each can be seamlessly derived from our unidirectional pulse propagation equation (UPPE).

Most of the pulse propagation problems in nonlinear optics are solved in one of two formulations: Either one has an initial condition (electric and magnetic fields) specified in all space, and the evolution is calculated along the time axis, or the initial condition is given as a function of local pulse time and transverse (w.r.t. propagation direction) coordinates, and the numerical evolution proceeds along the propagation axis. We refer to these cases as time- and z-propagated equations.

The z-propagated approach is much more common in nonlinear optics simulations based on envelope equations, often related to NLS. The time-propagated approach is on the other hand common for solvers based on direct integration of Maxwell's equations.

Due to space limitations, we focus in this article on the z-UPPE. The t-propagated version was originally introduced in reference [3]. As discussed in reference [2,3] in more detail, the time-propagated versions of UPPE are more suitable for tight-focusing scenarios when non-paraxial effects start to play a role. The z-propagated equations are easier to use in situations that allow one to neglect the longitudinal field components as sources of nonlinear material response.

We write down a simplified scalar version of z-UPPE for the transverse electric field components

$$\partial_z E_{k_x,k_y}(\omega,z) = ik_z E_{k_x,k_y}(\omega,z) + \left(\frac{i\omega^2}{2\varepsilon_0 c^2 k_z} P_{k_x,k_y}(\omega,z) - \frac{\omega}{2\varepsilon_0 c^2 k_z} j_{k_x,k_y}(\omega,z) \right) \qquad (2.1)$$

This is the most useful form for practical calculations, and is therefore called z-UPPE in the following. The polarization source term $P_{k_x,k_y}(\omega,z)$ and current density $j_{k_x,k_y}(\omega,z)$ are sources driving the field

Nonlinear Material Response

In most cases, the propagation equations discussed in this chapter do not require a specific form of material response. However, for the sake of concreteness, as well as for discussion of numerical methods, we want to describe a generic model of nonlinear material response. We consider a nonmagnetic, dispersive medium with relative permittivity ε that is a function of the transverse coordinates x,y and of the angular frequency ω

$$\varepsilon = \varepsilon(\omega,x,y), \quad \mu = \mu_0$$

This medium specification includes any dispersive homogeneous medium such as air or water as well as structured fiber-like media such as photonic, microstructured and tapered optical fibers.

Nonlinear effects are usually described in terms of polarization P through the material constitutive relation:

$$\vec{D} = \varepsilon_0 \varepsilon * \vec{E} + \vec{P}$$

The star in this formula represents a convolution integral with ε being the linear response function corresponding to the frequency dependent $\varepsilon(\omega, x, y)$. The non-linear polarization is an ``arbitrary" function of the electric field $\vec{P} = \vec{P}(\vec{E})$.

We will also include a current density that is driven by the optical field

$$\vec{j} = \vec{j}(\vec{E})$$

to describe interactions with plasma generated by the high-intensity optical pulse.

The main physical effects that influence propagation of ultrashort, high-power light pulses in nonlinear dispersive media include the optical Kerr and stimulated Raman effects, free-electron generation, defocusing by the generated plasma and losses caused by avalanche and multiphoton ionization (MPI). With minor modifications, models including these effects can be used for description of ultra-short optical pulses propagation in gases[4-20], condensed bulk media[21-25] and in conventional, microstructured, and tapered fibers[26-28] as well as in ultra-thin silica ``wires"[29].

The optical Kerr and stimulated Raman effects cause a local modification of the optical susceptibility

$$\vec{P} = \varepsilon_0 \Delta\chi \vec{E}$$

that responds to the history of the light intensity I:

$$\Delta\chi = 2 n_b n_2 \left[(1-f) I + f \int_0^\infty R(\tau) I(t-\tau) d\tau \right]$$

Here, f is the fraction of the delayed nonlinear response, and R(τ) is the memory function of the stimulated Raman effect. Parameterization by $R(\tau) \sim \sin(\Omega\tau) e^{-\Gamma\tau}$ is often sufficient for ultrashort pulses[30]. This simple formula has the advantage of easy implementation that avoids explicit calculation of the convolution integral. Often, an even simpler, exponential memory function is used, $R(\tau) \sim e^{-\Gamma\tau}$ in simulations[31]. If the real memory function is sufficiently complex, a numerical convolution approach must be used to calculate the convolution. This is e.g. the case in silica[32].

Because of the potentially high intensities occurring in femtosecond pulses, free electrons are generated by MPI and avalanche mechanisms. Then it is necessary to account for the response of the optical field to the presence of a dilute plasma. Since the relevant times scales are so short, plasma diffusion and ion motion are neglected, and the free-electron density ρ is usually obtained as a solution to an equation of the following form[14,15,30]

$$\partial_t \rho = aI\rho + b(I) - c\rho^2$$

Here, I is the light intensity, a parameterizes the avalanche free-electron generation, and b(I) represents the multi photon ionization (MPI) rate that is a highly nonlinear function of the intensity. The last term describes plasma recombination. More realistic MPI rates can be calculated using ab initio time-dependent S-matrix theory for example.

We assume that the collective electron velocity $\vec{v}$ responds to the optical field and that the total current density is governed by the following simple equation[33]

$$\frac{d}{dt}\vec{j}(t) = \frac{e^2}{m_e}\rho(t)\vec{E}(t) - \vec{j}(t)/\tau_c$$

where τ_c is the mean time between collisions experienced by electrons. This equation is solved together with the above equation for ρ to capture effects of the plasma on the propagation of the optical field, namely defocusing due to plasma and plasma induced losses.

Losses caused by multiphoton ionization are usually incorporated as either an equivalent current[34,35] or an imaginary susceptibility contribution that extracts from the field the energy needed for the free-electron generation.

3. DERIVATION OF OTHER NONLINEAR ENVELOPE EQUATIONS

Several types of unidirectional propagation equations are widely used in the nonlinear optics literature. The most important examples are Non-Linear Schrödinger (NLS) equation[36], Nonlinear Envelope Equation[37] (NEE), the First-Order Propagation equation[35] (FOP), Forward Maxwell's equation[38] (FME), and several other equations that are closely related to these. In this section, we provide a unified approach that will be used to derive several of the light-pulse propagation equations found in the literature. The main benefit of re-deriving known equations from a common starting point, namely UPPE, using the same method, is that it allows us to compare the physical assumptions and approximation underlying different equations.

It is instructive to break the derivation procedure into several steps. As a first step, we adopt a scalar, one component approximation and write the UPPE in the following form:

$$\partial_z E_{k_x,k_y}(\omega,z) = iKE_{k_x,k_y}(\omega,z) + iQP_{k_x,k_y}(\omega,z) \tag{3.1}$$

where

$$K(k_x,k_y,\omega) = \sqrt{\omega^2\varepsilon(\omega)/c^2 - k_x^2 - k_y^2}$$

is the linear field propagator in the spectral representation, and

$$Q(k_x,k_y,\omega) = \frac{\omega^2}{2\varepsilon_0 c^2\sqrt{\omega^2\varepsilon(\omega)/c^2 - k_x^2 - k_y^2}}$$

will be called nonlinear coupling term.

In the second step, we replace K and Q by suitable approximations. In most cases they are nothing but Taylor expansions in frequency and in transverse wavenumber.

To obtain envelope equations, one expresses the field in terms of an envelope by factoring out the carrier wave at a chosen reference angular frequency ω_R with the corresponding wave-vector $k_R = K(0,0,\omega_R)$

$$E(x,y,z,t) = A(x,y,z,t)e^{i(k_R z - \omega_R t)} \tag{3.2}$$

A similar factorization is of course introduced for the nonlinear polarization P(x,y,z,t) as well.

Step three consists of transforming the equation from the spectral- to the real-space representation. Mathematically, this is nothing but a Fourier transform that results in the following standard rules for differential operators:

$$(\omega-\omega_R) \leftrightarrow i\partial_t \quad ik_x \leftrightarrow \partial_x \quad ik_y \leftrightarrow \partial_y \quad i(k(\omega_R)-k_z) \leftrightarrow \partial_z \tag{3.3}$$

Finally, in most cases we also transform to a frame moving with a suitable group velocity such that the pulse remains close to the center of the computational domain.

Derivation of Non-Linear Schrödinger Equation from UPPE

The Nonlinear Schrödinger Equation[36] (NLS) is the computational workhorse for ultrashort pulse propagation and has been used extensively to model atmospheric light string propagation. One characteristic feature of NLS and of other envelope type equations is the presence of a reference frequency. Usually, one chooses the reference angular frequency ω_R as the central frequency of the initial pulse, but this is not necessary. Actually it is useful to keep in mind that ω_R is to a certain extent a free parameter, and that the obtained results must be almost independent of its concrete choice. If a numerical simulation turns out to be sensitive to the choice of ω_R, it means that an envelope equation is being used outside of its region of validity.

Following the general procedure, we replace the K and Q ``coefficients" with appropriate approximations. We denote by $k_R=k(\omega_R)$ the reference wavenumber corresponding to the chosen reference frequency ω_R, and take

$$K(k_x,k_y,\omega) = \sqrt{\omega^2\varepsilon(\omega)/c^2 - k_x^2 - k_y^2} \approx k_R + v_g^{-1}(\omega-\omega_R) + \frac{k''}{2}(\omega-\omega_R)^2 - \frac{1}{2k_R}(k_x^2+k_y^2)$$

This is a second-order Taylor expansion in ω-ω_R and in k_x, k_y.

In the nonlinear coupling coefficient, we neglect all variable dependencies and take its value at the reference frequency and zero transverse wavenumber:

$$Q\left(k_x,k_y,\omega\right)=\frac{\omega^2}{2\varepsilon_0 c^2\sqrt{\omega^2\varepsilon\left(\omega\right)/c^2-k_x^2-k_y^2}}\approx\frac{\omega_R}{2\varepsilon_0 n\left(\omega_R\right)c}$$

For simplicity, in NLS we only account for the instantaneous optical Kerr effect, and write the nonlinear polarization envelope as

$$P=2\varepsilon_0 n\left(\omega_R\right)n_2\,|\,A\,|^2\;A$$

Inserting the above expressions into equations (3.1), (3.2) we obtain

$$\partial_z A=iv_g^{-1}\left(\omega-\omega_R\right)A+i\frac{k''}{2}\left(\omega-\omega_R\right)^2 A-\frac{i}{2k_R}\left(k_x^2+k_y^2\right)A+i\frac{\omega_R}{c}n_2\,|\,A\,|^2\;A$$

It is customary to normalize the envelope amplitude such that $|\{A\}|^2 = I$. Using rules given by equation (3.3) we finally obtain the NLS equation:

$$\left(\partial_z+v_g^{-1}\partial_t\right)A=\frac{i}{2k_R}\nabla_T^2 A-i\frac{k''}{2}\partial_{tt}A+i\frac{\omega_R}{c}n_2\,|\,A\,|^2\;A$$

Approximating K to second order in frequency and transverse wavenumber amounts to the paraxial, and quasi-monochromatic approximations for the linear wave propagation. The approximation in the nonlinear coupling Q also requires a narrow spectrum in order to be able to represent Q by a constant.

Derivation of the Nonlinear Envelope Equation

The Nonlinear Envelope Equation[37] is a paraxial equation with some additional approximations related to chromatic dispersion. This equation appears to be extremely close to the paraxial version of UPPE.

Once again we follow the general procedure and approximate the linear propagator by its paraxial version:

$$K\left(k_x,k_y,\omega\right)=\sqrt{\omega^2\varepsilon\left(\omega\right)/c^2-k_x^2-k_y^2}\approx k\left(\omega\right)-\frac{c}{2\omega n\left(\omega_R\right)}\left(k_x^2+k_y^2\right)$$

This is essentially the second-order (paraxial) Taylor expansion in transverse wavenumber with only minor additional approximation. Namely, we replaced $n_b(\omega) \rightarrow n_b(\omega_R)$ in the denominator of the diffraction term, and thus partly neglected the chromatic dispersion.

Further, the first term in the above approximation, which is an exact propagation constant for a plane wave propagating along the z axis, is re-expressed as a sum of its two lowest-order Taylor expansion terms plus the rest:

$$k\left(\omega\right)=k\left(\omega_R\right)+v_g^{-1}\left(\omega-\omega_R\right)+D\left(\omega-\omega_R\right)$$

where

$$D\left(\omega-\omega_R\right)=\sum_{n=2}^{\infty}\left(\frac{\partial^n k}{\partial\omega^n}\right)_{\omega=\omega_R}\frac{\left(\omega-\omega_R\right)^n}{n!}$$

This is formally exact and can be practically implemented in the spectral domain without further approximations, but sometimes a finite number of series expansion terms is used to fit the linear chromatic dispersion of a medium or of a waveguide. What we understand under NEE in the following assumes an exact treatment of the dispersion operator.

Next, we approximate the nonlinear coupling term. Unlike in NLS, we preserve the frequency dependence exactly, but neglect the transverse wave-number dependence:

$$Q\left(k_x,k_y,\omega\right)=\frac{\omega^2}{2\varepsilon_0 c^2\sqrt{\omega^2\varepsilon(\omega)/c^2-k_x^2-k_y^2}}\approx\frac{(\omega-\omega_R)+\omega_R}{2\varepsilon_0 n(\omega_R)c}$$

Here, as in the free propagation term, we neglect the chromatic dispersion of the background index of refraction.

After putting the above approximations for K and Q into the original UPPE, we obtain

$$\partial_z A=iv_g^{-1}(\omega-\omega_R)A+iD(\omega-\omega_R)A-\frac{ic}{2\omega_R n(\omega_R)}\left(1+\frac{(\omega-\omega_R)}{\omega_R}\right)^{-1}\left(k_x^2+k_y^2\right)A \qquad (3.4)$$

$$+\frac{i\omega_R}{2\varepsilon_0 cn(\omega_R)}\left(1+\frac{(\omega-\omega_R)}{\omega_R}\right)P$$

Finally, transforming into the real-space representation, we arrive at NEE

$$\partial_z+v_g^{-1}\partial_t A=iD(i\partial_t)A+\frac{i}{2k_R}\left(1+\frac{i}{\omega_R}\partial_t\right)^{-1}\nabla_T^2 A+\frac{ik_R}{2\varepsilon_0 n_b^2(\omega_R)}\left(1+\frac{i}{\omega_R}\partial_t\right)P$$

Thus, the additional approximations underlying the NEE are paraxiality both in the free propagator and in the nonlinear coupling, and a small error in the chromatic dispersion introduced when the background index of refraction is replaced by a constant, frequency independent value in both the spatio-temporal correction term and in the nonlinear coupling term.

A partially Corrected NLS (PC-NLS) equation can be viewed as a ``simplification" of NEE. It is derived from the UPPE in the same way, with one additional step. Namely, the following first order series expansion is applied in the correction term of the free propagator in equation (3.4):

$$\left(1+\frac{\omega-\omega_R}{\omega_R}\right)^{-1}\simeq\left(1-\frac{\omega-\omega_R}{\omega_R}\right)$$

This approximation step is meant to make it easy to implement a

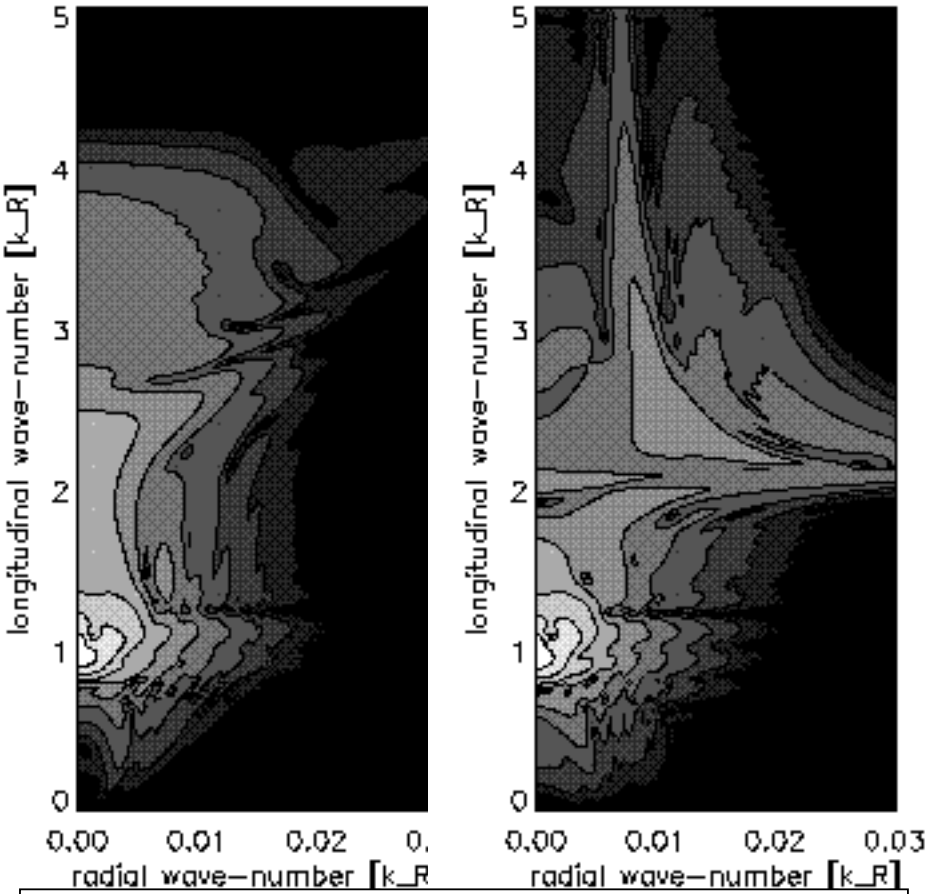

Figure 1 Spectrally-resolved far-field of the generated white-light SC showing wavelength and angular resolved spectrum. Left: z-UPPE. Right: PC-NLS

numerical solver in real space, as it results in the equation that only contains ``simple" differential operators in the real-space representation:

$$\partial_z + v_g^{-1}\partial_t A = iD(i\partial_t)A + \frac{i}{2k_R}\left(1 - \frac{i}{\omega_R}\partial_t\right)\nabla_T^2 A + \frac{ik_R}{2\varepsilon_0 n_b^2(\omega_R)}\left(1 + \frac{i}{\omega_R}\partial_t\right)P$$

While it may seem that the Partially Corrected NLS is essentially NEE with a ``little more" approximation, this equation is not to be recommended. Because of the arbitrary truncation of an infinite series, the dispersion properties of the linear part of this equation are unphysical. While the PC-NLS provides better-than-NLS approximation around the reference frequency ω_R, its dispersion properties become rather pathological around $\omega \simeq 2\omega_R$ where its diffraction term changes sign as a consequence of the truncated correction factor. Artifacts in the angular distribution of the spectrum can be observed at high frequencies beyond $\omega \simeq 2\omega_R$. This is illustrated in Figure 1. Consequently, this equation is only applicable in the same regime as the NLS, namely when the spectrum of the pulse remains relatively narrow.

4. LIGHT STRING GENERATION

The qualitative behavior of intense pulse propagation in the atmosphere can be most transparently captured by extending the usual Nonlinear Schrödinger propagation model to include coupling to a simple Drüde model that describes generation of an electron-ion plasma[9].

$$\frac{\partial A}{\partial z} = \frac{i}{2k}\nabla_T^2 A - i\frac{k''}{2}\frac{\partial^2 A}{\partial t^2} + ikn_2 |A|^2 A - \frac{\sigma}{2}(1 + i\omega\tau)\rho A - \frac{\beta^{(N)}}{2}|A|^{2N-2}$$

$$\frac{\partial \rho}{\partial t} = \frac{1}{n_b^2}\frac{\sigma}{E_g}\rho |A|^2 + \frac{\beta^{(N)}}{N\hbar\omega}|A|^{2N} - a\rho^2$$

The first three terms on the RHS of the first equation account for diffraction, temporal dispersion and Kerr self-focusing. The remaining terms in this first equation describe plasma absorption/dispersion respectively and losses due to multi-photon absorption. In air propagation, the order of multiphoton ionization is 7 for N_2 and 8 for O_2. Thus the multi-photon ionization is of much higher order than the Kerr self-focusing. Moreover, the refractive contribution to the plasma term is about two orders of magnitude greater than the absorptive term, meaning that dissipation per self-focusing event is small relative to the induced negative lens. The second equation is a simple Drüde model to account for free electron/ion generation through avalanche photo-ionization (first term in second equation) and multi-photon generation (second term). The latter term accounts for recombination losses. The femtosecond pulse interaction with air is so fast that avalanche ionization and recombination can be ignored – likewise we ignore plasma drift and diffusion processes.

Multiple Filament Formation across wide pulses

This first application of the z-UPPE simulator illustrates break-up of a high-power, wide femtosecond pulse into chaotically interacting light filaments. Beams that carry power far exceeding the critical self-focusing power usually break-up transversally into multiple filaments. For air, $P_{crit} \approx$ 4-5 GW suggesting that a few TW pulse could contain on the order of one thousand filaments – in practice, numerical simulations and experimental measurements indicate that about 10-15% of the total power is concentrated in filaments (light strings) at one time. Figure 2 shows an experimental energy fluence profile of a few TW pulse creating filaments (light strings) in air. The bright localized spots represent focused high-intensity light strings. To capture such dynamics, a fully spatially resolved simulator is needed that doesn't impose axial symmetry.

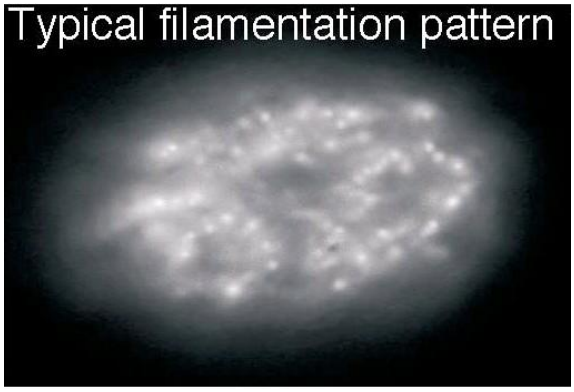

Figure 2 Experimentally measured energy fluence profile of a high power pulse propagating in air. **[**K. Stelmaszczyk et al. APL, **85**, 3977 (2004)]

We illustrate in Figure 3 how multiple filaments are concurrently

created at different transverse and longitudinal locations, and how they interact with the low-intensity background. It was first proposed in reference [17] that such an interaction is crucial for long distance propagation of high-power femtosecond pulses in air. The basic idea is that of dynamic exchange of energy between multiple, essentially unsynchronized and spatially sharply localized filament cores and the low-intensity, spatially wide pedestal of the beam.

In this wide-beam simulation, the initial condition is a Gaussian pulse with a phase perturbation. The waist of the initially collimated Gaussian was chosen to be 5mm, the pulse duration is 500 fs, $\lambda = 248\,\text{nm}$, and the maximal intensity is $2\times10^{14} Wm^{-2}$. The total pulse energy is approximately 9mJ. A random phase perturbation is imposed on the pulse to initiate the transverse break-up of the pulse into multiple filaments (see Figure 3). We adjusted the amplitude of the perturbation such that it results in the filamentation onset after a few meters of propagation. The numerically computed filaments show the same qualitative features as the experimental measurements in Figure 2.

The first stage of nonlinear self-focusing is driven by the smooth, large-scale profile of the pulse. After a few meters, local perturbations develop into hot-spots which grow into high-intensity filaments. The first panel shows the overall scale of the input pulse with the high-intensity regions forming from the low-intensity background. There is practically no plasma formation at this propagation distance. The initial perturbations grow rapidly and reach intensities high enough to ionize air (second panel). Collapse of a filament is eventually regularized by plasma-induced defocusing. That causes decay of the filament and returns most of its energy into the low-intensity background. From there, new filaments grow and these replenishment cycles repeat with relatively modest energy losses to plasma generation (subsequent panels).

Later in the propagation, filaments start to appear in the peripheral regions further from the center. This is due to less overall intensity and therefore slower self-focusing and growth of perturbations. Though it is not evident on these fluence pictures, later-stage filaments tend to generate less plasma than the ones that appear at the very beginning of the filamentation onset. This is the stage when the single-filament dynamic spatial replenishment scenario crosses over to a regime where replenishment energy originates in ``neighboring" filaments rather than from the same one.

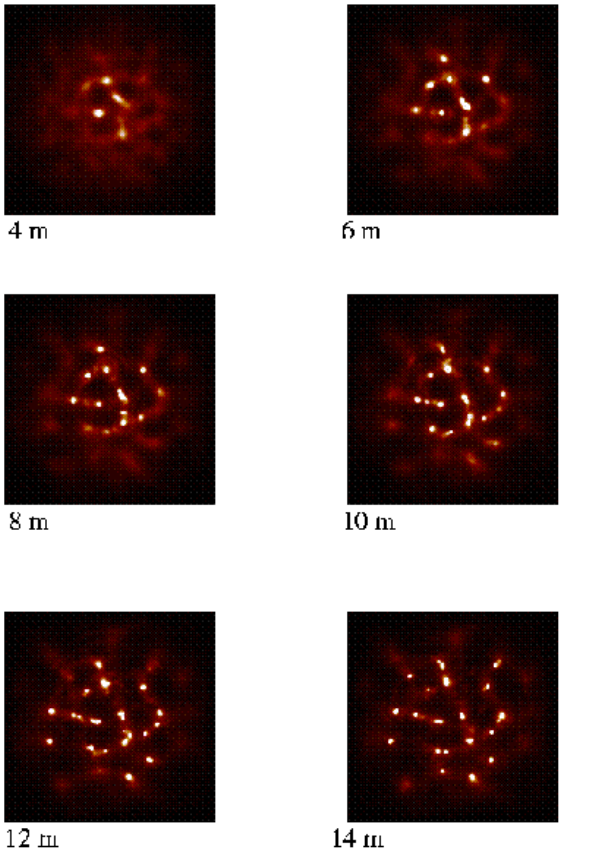

Figure 3 Transverse energy fluence profiles at different propagation distances. White colors represent most intense light filaments.

Initial sharp spikes in the total number of generated electrons, associated with the onset of individual filaments, decay with distance. We expect the shot-to-shot fluctuation to smooth-out these sharp features due to randomization of the filament formation. The late-stage filaments are less ``organized" than those created just after the self-focusing onset. Consequently, it takes less of the plasma generation to arrest their collapse. One can say that the increasing ``disorder" in the developing composite pulse makes the collapse arrest due to plasma more efficient and thus contribute to the ability of the pulse to propagate over long distances. One can speculate, and recent experiments indicate that a regime can be eventually reached where the plasma generation is almost negligible.

A number of recent experiments on light string propagation in air have addressed the issue of competition between SC generation and third harmonic generation (THG)[39,40]. In a tightly (linearly) focused geometry, it has been observed that the spectral extent of SC generation is quite limited and a third harmonic signal can be clearly seen as a separate isolated spectral component. This situation falls within the classical NLO description of THG where, one can describe the fundamental and third harmonic waves as separate, coupled slowly varying envelopes. In a loosely focused geometry however, where the propagating pulse is allowed to spontaneously self-focus, the situation is very different. The onset of critical self-focusing

generates explosive SC prior to the local intensity being reached where significant THG can be seen. Consequently, the SC spectrum rapidly swamps the THG signal. In this case one cannot think in terms of isolated envelope waves and must include the full electromagnetic field[41].

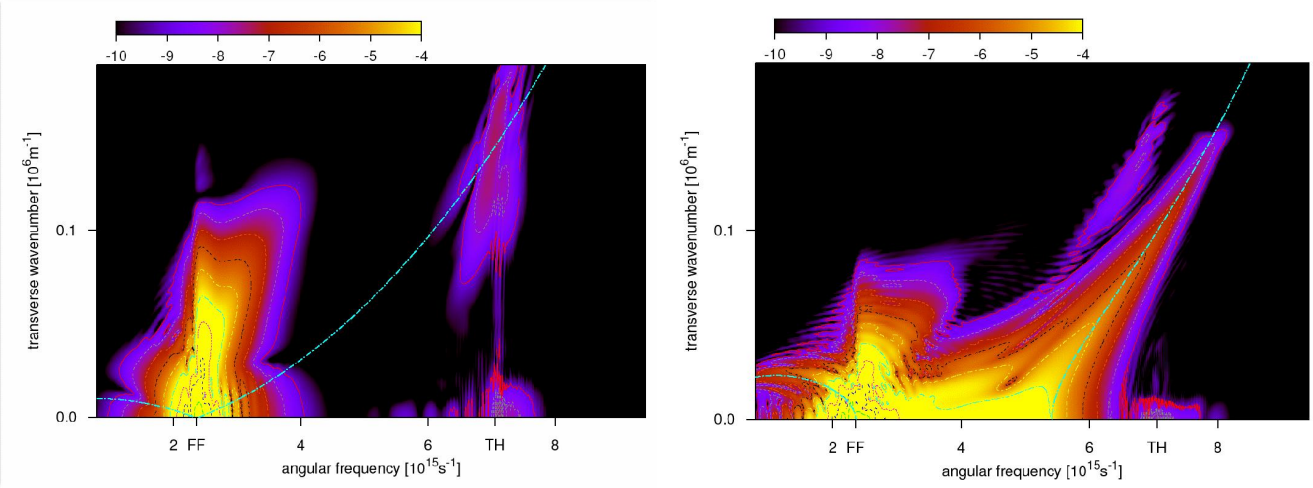

Figure 4 Left panel: Spectrally resolved far-field showing the spectral content of the fundamental (FF) and the third harmonic (TH) after propagation in a tightly focused geometry. Dashed curve is the locus of the dynamic THG phase-matching condition. Right panel: Corresponding spectrally resolved far-field for propagation in a loosely focused geometry.

Figure 4 shows the spectrally resolved far-field spectra for both situations. In the tightly focused geometry, on the left panel, the spectrum shows a strong angular divergence (vertical axis) about the fundamental but remains essentially isolated from the third harmonic. The third harmonic signal contains energy concentrated on-axis and off-axis near the phase matching curve. The latter appears as THG emission in a concentric ring about the fundamental. The on-axis signal contains a mix of fundamental and THG. In the loosely focused geometry, the pulse propagates some distance in air before undergoing explosive critical self-focusing. At the onset of critical-self focusing, there is strong SC generation and the spectrum broadens dramatically. In fact, the SC spectrum swamps the THG signal but aligns itself dominantly along the THG phase matching curve.

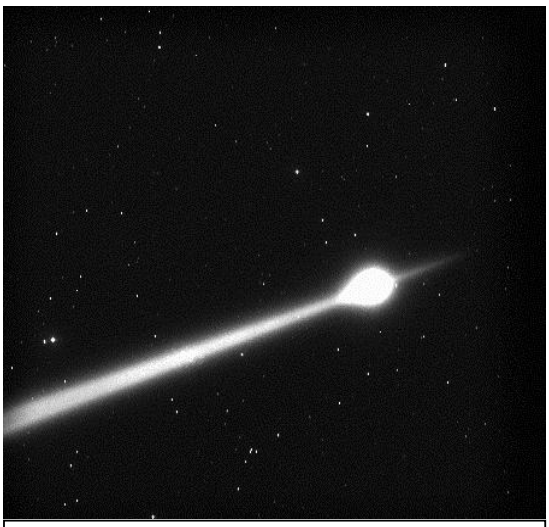

Figure 5 White-light supecontinuum propagating vertically in the atmosphere. White dots are stars in the background.

Applications of Light Strings

Multi-terawatt pulses with carrier wavelength in the infra-red (λ = 800 nm) and typically lasting for 100-200 fs have been employed by the Teramobile group as a novel fs Lidar system[42]. Detected light using an imaging 2-m telescope has been observed from altitudes exceeding 20 km vertically in the atmosphere. Direct observation in several wavelength bands supports filament formation at distances as far as 2 km in the atmosphere. Moreover the beam divergence at 5 km altitude is smaller than expected supporting whole-beam waveguiding. The high local intensities accompanying light string formation lead to the generation of intense white-light SC – the latter has been observed propagating at ranges exceeding 18 km vertically in the atmosphere (see Figure 5). These experimental observations have created new perspectives for white-light Lidar (light detection and ranging). Plasma channels generated with light strings have been shown to guide high-voltage discharges between electrodes making them potential candidates for lightning control.

Both theoretical simulations and experimental measurements indicate individual light strings and plasma channels persist over meter lengths. Recent experiments even suggest that plasma channels can extend up to 400 m when using multi-terawatt laser pulses. The high density of such light strings across a TW pulse and their chaotic generation and regeneration ensures that the effective propagation length is much longer. Indeed recent experimental measurements suggest that two distinct propagation regimes exist – an initial scenario involving relatively violent critical self-focusing collapse across the wide pulse with concomitant plasma generation (detected by THz emission) followed by a relatively quiescent regime where light strings persist longer and generate less or no plasma. This latter behavior has not been satisfactorily explained theoretically so far.

Another important application scenario for light strings is so-called remote Laser-Induced-Breakdown-Spectroscopy (LIBS)[43]. The persistence of light strings and associated plasma channels over meter long distances and their chaotic generation and regeneration considerably relaxes the stringent focusing requirements of conventional LIBS. In the latter, an intense laser pulse must be focused close to the target – otherwise the pulse will have spread diffractively and no plasma can be generated. Light string sources provide a statistical sampling of the target within a single pulse and do not require special focusing conditions. This latter fact considerably extends the flexibility and range of remote LIBS for remote chemical identification and chemical analysis. The Teramobile system was used to induce ablation on a metal target at a distance greater than 100 m away – based on these results a remote LIBS detection system is proposed that would operate at kilometer ranges. Figure 6 shows a comparison of the range corrected signal using light strings. It is seen to be relatively insensitive to distance variation in contrast to the classical LIBS approach where the signal falls off rapidly beyond the linear focus.

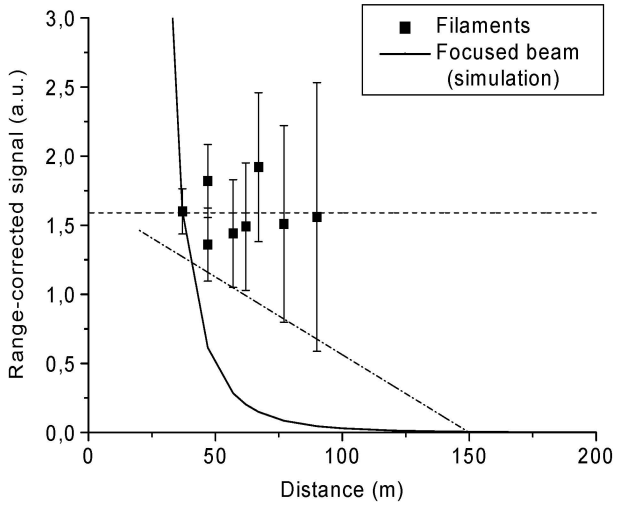

Figure 6 Range-corrected signal using remote LIBS spectroscopy on a metal target. The continuous line is a simulation of classical LIBS. [K. Stelmaszczyk et al. APL, **85**, 3977 (2004)]

5. NONLINEAR X- AND O-WAVES IN WATER

Weakly focused femtosecond laser pulse propagating in water can exhibit novel self-trapping over distances of a few centimeters. While there are many analogies with propagation in air there are importance difference also. The characteristic transverse size of light strings in air is limited to about a 100 μm diameter due to the onset of optical breakdown. This means that air propagation is mostly near-paraxial. In air propagation, dispersion is not a major player whereas it plays a prominent role in water. The strong interplay between transverse self-focusing compression and strong linear dispersion in water leads to dominant non-paraxial propagation effects. Depending on whether the optical carrier wave of the exciting pulse is in the normal or anomalous region of the water dispersion, the nonlinear focusing behavior can be quite different. Water has the nice property that its optical properties are well characterized and hence, it provides an ideal medium for validating our UPPE solver.

Figure 7 shows measured absorption and dispersion features of water over a broad span of wavelengths. An exciting pulse at 527 nm will exhibit normal GVD whereas a pulse at 1100 nm experiences anomalous GVD. This particular example requires that the solver captures correctly the linear dispersion in a broad range of frequencies and propagation angles, and is thus an ideal candidate for UPPE application. Full details can be found in an earlier publication[44]. The dots in the right picture represent experimental GVD data and the continuous curve the corresponding effective dispersion of the numerical algorithm – in other words, the UPPE propagator captures the real physical dispersion (and absorption) over the full bandwidth shown in this figure.

Firstly we consider a loosely focused femtosecond pulse centered at a 527~nm wavelength, propagating in a water sample. An appropriate combination of focusing, pulse intensity and duration results in a long filament (compared to the Rayleigh range corresponding to the transverse size of the beam at the water-cell entrance). The question that we want to shed light on in this numerical experiment is what mechanism is responsible for creation of that seemingly several centimeters long filament. Further, we want to know if the mechanism is universal in any way.

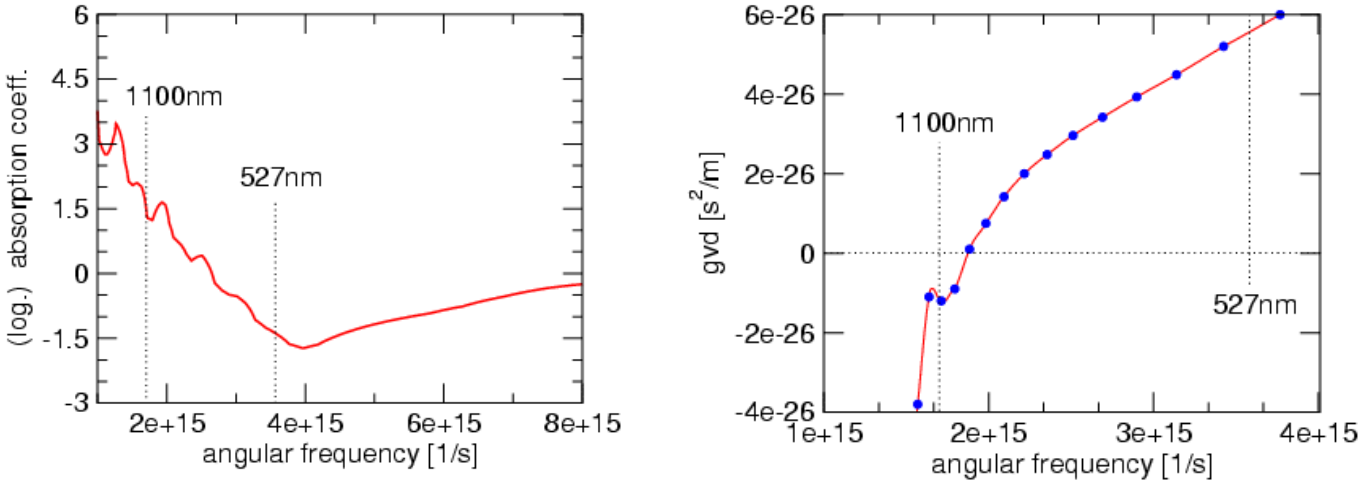

Figure 7 Left: Water absorption spectrum on a log scale. Right: Corresponding group velocity dispersion (GVD). The vertical lines indicate the carrier wavelength corresponding to anomalous (1100 nm) and normal (527 nm) dispersion.

It is important to note that what is actually observed, in experiment[45,46] and in simulation[47] alike, is not a ``steady-state" self-guided filament. Rather, we deal with a series of pulse splitting events akin to the scenario of spatial dynamical replenishment[30] in air. In this case, however, the role of plasma as the arrestor of the self-focusing collapse is less pronounced compared to propagation in air. The left and center panels of Figure 8 show a series of snapshots that depict the temporal profile of on-axis intensity of the now quite complicated ``pulse." One observes several cycles consisting of formation and subsequent splitting of a sub-pulse in the center of the time domain. The ``daughter" sub-pulses resulting from each pulse-

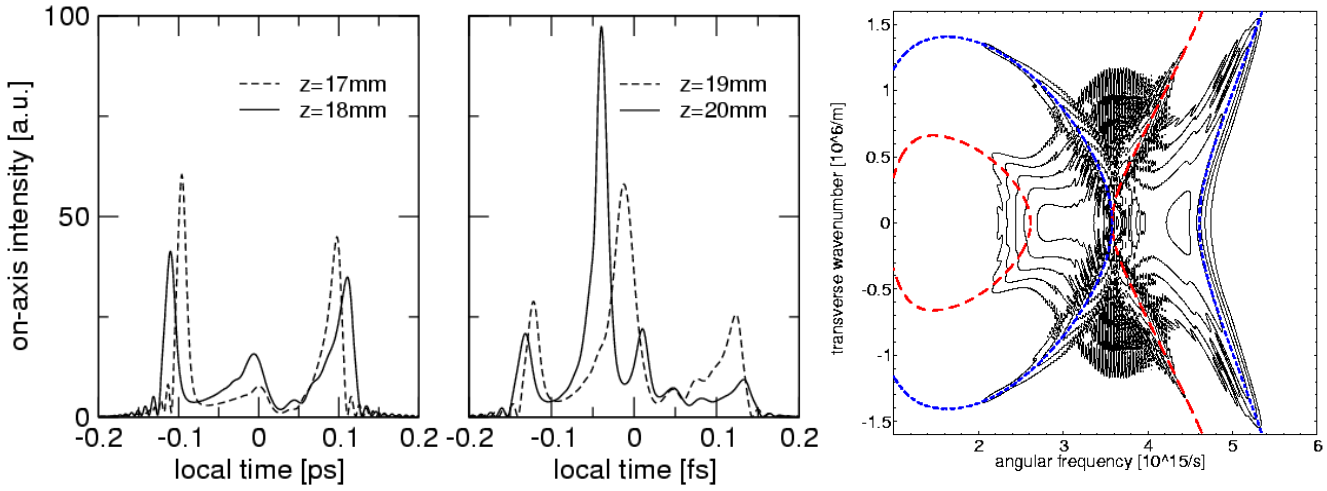

Figure 8 The left and center picture show snapshots of 1D slices through the 3D pulse at different propagation distances in water. The picture on the right is the spectrally-resolved far-field showing the characteristic X-feature in the accumulated spectrum. The dashed lines are loci of a dynamic 3-wave mixing formula.

split event play an important role in the formation of the spatial and temporal spectrum. Namely they are still intense enough to induce localized changes to the material susceptibility that in turn follow these split-off pulses and thus propagate with different ``group" velocities. These material waves then act as scatterers in a three-wave mixing process that transforms the input optical waves into scattered ones. Linear propagation dispersion properties together with the propagation velocity of the material wave then determine where in the spectral space the scattered energy will accumulate.

The dashed lines in the right panel of Figure 8 represent the loci of spectral energy concentration predicted from an effective three-wave mixing argument. The resulting spatio-temporal spectrum of a loosely focused ultrashort pulse after propagation in water is shown in Figure 8 The dashed lines represent the loci where energy concentrates due to the non-linear interactions irrespective of the details of the underlying dynamics. The resulting central X-shaped feature is always close to the manifold that supports the z-invariant X-waves that propagate long distances without changing their spatio-temporal spectral shapes. In any normal-GVD medium, the ``theoretical X-wave" spectrum and the ``real-pulse" spectral concentration will be close to each other because of the simple landscape of chromatic dispersion in the space of frequency and transverse wavenumber. Thus, even highly non-stationary pulses inherit their tendency for long-distance propagation from the nonlinear X-waves. This global robust feature of nonlinear X-waves has been observed experimentally in recent experiments [45,46]. What is quite remarkable is that there appears to be a universal attracting set in the infinite-dimensional phase space that attracts all solutions despite the extremely chaotic spatio-temporal evolution of the underlying dynamics. It is important to recognize that the 1D slices in Figure 8 are not fully representative of the complex underlying spatio-temporal dynamics that these self-trapped pulses undergo while self-trapped.

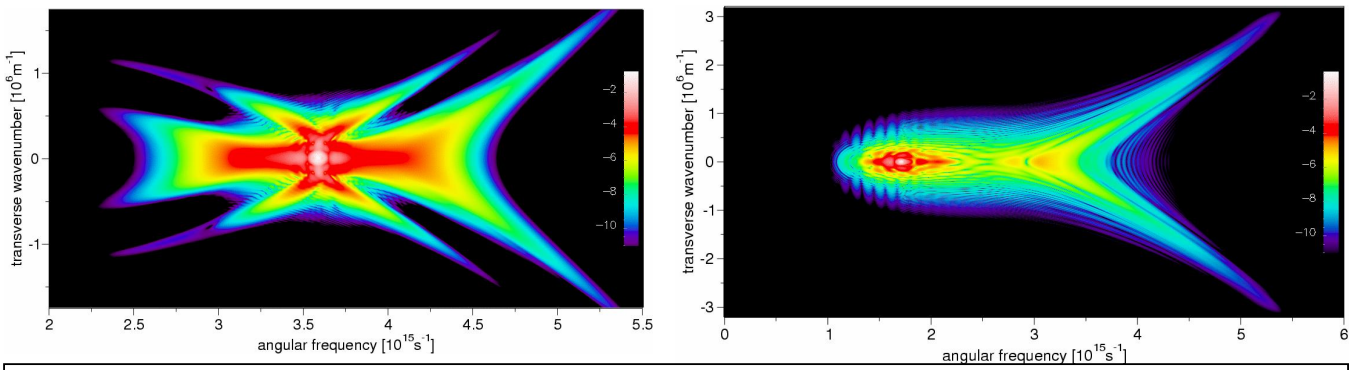

Figure 9 Left panel: Spectrally-resolved far field for the pulse carrier wavelength in the normal dispersion regime of water. Right panel: Spectrally-resolved far-field for the pulse carrier wavelength in the anomalously dispersion regime.

By changing the central pulse wavelength to 1100 nm we access the anomalous dispersion regime of water (see Figure 7). Notice however that the zero dispersion cross-over to normal dispersion is much closer to this wavelength. When a pulse is launched in water at this wavelength, it experiences anomalous dispersion. Hence, there is now a tendency to contract the pulse in both the transverse dimension (self-focusing counteracting diffraction) and in the longitudinal dimension (self-focusing counteracting dispersion). This scenario where contraction occurs in all three dimensions is called supercritical collapse. The accumulated spectrally resolved far-field spectrum now looks very different. Instead of an X-feature, one expects to see families of ellipses in the far-field spectrum reflecting the dominance of the 3D linear dispersion landscape. Because of the relative closeness of the 1100 nm wavelength to the zero dispersion cross-over point, we observe that the SC expands into the normal dispersion regime of the water response leading to a part X-feature at short wavelengths. Figure 9 shows the X-wave spectrally -resolved far-field in the left panel and the O-wave spectrally-resolved far-field in the right panel. The strong off-axis flow of energy in these spectra is indicative of non-paraxial behavior and, coupled with extreme SC generation, requires a UPPE level solver for proper resolution.

CONCLUSIONS

In this article, we have presented an overview of some recent exciting experimental developments in the field of intense ultrashort pulse propagation effects in the atmosphere and in water. Atmospheric light string generation and propagation with multi-TW 100-200 fs duration laser pulses has opened up a whole new vista of novel applications areas involving long distance propagation effects. We have seen that intense light strings created chaotically within the laser pulse can generate a remote white-light continuum spectroscopic probe in the atmosphere. They also leave behind dilute plasma channels that have direct use in a new form of remote LIBS spectroscopy and the latter can emit THz radiation. Of course, the atmosphere is not a well-controlled laboratory environment and we can only hope to get qualitative understanding of such highly nonlinear propagation phenomena. Some recent experimental studies of self-trapping of ultra-short laser pulses in water have identified some novel consequences of the coupling between diffraction, dispersion and nonlinear self-focusing. Nonlinear X-waves, which are somewhat related to linear non-diffracting Bessel beams have been observed when the laser carrier wavelength is in the normal region of the water response while O-waves are observed in the anomalous dispersion region.

An underlying theme of the article has been the importance of having a physically realistic theoretical description and numerical implementations that capture the relevant physics over the very broad spectral landscape experiencing nonlinear excitation. We pointed out that the famous NLS equation, when extended to account for plasma generation, can give a very useful qualitative description of the important physical mechanisms operative during intense ultra-short pulse propagation. The need for a more complete model was emphasized and we presented a carrier resolved unidirectional vector Maxwell propagator (z-UPPE) that allows for 3D pulse propagation over many meter distances. Full details of the alternate t-UPPE model are contained in references [2,3]. In addition to their computational feasibility, the UPPE models provide the first unified and seamless approach to deriving other envelope equation propagators in the literature. The physical approximations made in each envelope model are made explicit and these can be tested against the full UPPE.

A significant shortcoming of all existing nonlinear EM propagation models, including vector Maxwell, are the rather naïve and crude material models being employed The latter are typically limited to spectrally narrow windows of the linear optical response even through many nonlinear optical propagation scenarios involve generation of super-broadened spectral features over many decades of wavelengths. Typically, we can do a reasonably good job of extending linear response functions to ultra-wide bandwidth but the nonlinear response description is a completely open question. Given the complex and highly nonlinear nature of light interaction of materials with intense femtosecond and sub-femtosecond optical pulses, it is clear that there has be a significant investment of effort in deriving computationally accessible nonlinear response functions in the future.

ACKNOWLEDGEMENTS

The author would like to thank Miroslav Kolesik and Ewan Wright of the College of Optical Sciences, University of Arizona for their continued active involvement and encouragement during the course of the work outlined in this paper. The author is particularly indebted to Dr. Arje Nachman of the U.S Air Force Office of Scientific Research (AFOSR) for his continued support of this work. Funding support is acknowledged from the Air Force Office of Scientific Research under grants: AFOSR F49620-02-1-0194 and AFOSR F49620-02-1-0355. Finally, the author wishes to acknowledge the very generous support of the Alexander von Humboldt Foundation (Germany) for their very generous support during a sabbatical leave.

REFERENCES

1. S.-W Bahk et al, Opt. Lett. **29** 2837 (2004)
2. M. Kolesik and J.V. Moloney, Phys. Rev. E **70**, 036604 (2004)
3. M. Kolesik, J.V. Moloney and M. Mlejnek, Phys. Rev. Lett., **89**, 283902 (2002)
4. A. Braun et al., Opt.Lett., **20**, 73 (1995)
5. A. Brodeur et al., Opt. Lett., **22**, 304 (1997)
6. H.R.Lange et al., Opt. Lett., **23**, 120 (1998)
7. E.T.J. Nibbering et al., **21**, 62 (1996)
8. O.G. Kosereva et al, Opt. Lett., **22**, 1332 (1997)
9. M. Mlejnek et al., Opt. Lett., **23**, 382 (1998)

10. B. La Fontaine et al., Phys. Of Plasmas, **6**, 1615 (1999)
11. M. Mlejnek et al., Phys. Rev. E, , **58**, 4903 (1998)
12. J. Schwarz et al., Opt. Commun., **180**, 383 (2000)
13. A. Chiron et al., Eur. Phys. J., D **6**, 383 (1999)
14. A. Couairon and L. Berge, Phys. of Plasmas, **7**, 193 (2000)
15. L. Berge and A. Couairon, Phys. of Plasmas, **7**, 210 (2000)
16. S. Petit et al., Opt. Commun., **175**, 323 (2000)
17. M. Mlejnek et al., Phys. Rev. Lett., **83**, 2938 (1999)
18. A. Talebpour et al., Opt. Commun., **171**, 285 (1999)
19. J.V. Moloney et al., Chaos, **10**, p559 (2000)
20. N. Aközbek et al., Phys. Rev. E, **61**, 4540 (2000)
21. J. Noack and A. Vogel, IEEE J. Quant. Electron., **35**, 1156 (1999)
22. S. Tzortzakis et al., Phys. Rev. Lett., **87**, 213902 (2001)
23. M. Kolesik et al., Phys. Rev. Lett., **91**, 043905 (2003)
24. M. Kolesik et al., Appl. Phys. B., **77**, 185 (2003)
25. W. Liu et al., Opt. Commun., **202**, 189 (2002)
26. J.M. Dudley and S. Coen, Opt. Lett., **27**, 1180 (2002)
27. J.M. Dudley et al., J. Opt. Soc. Am. B, **19**, 765 (2002)
28. A.L. Gaeta, Opt. Lett., **27,** 924 (2002)
29. L.Tong et al., Nature, **426**, 816 (2003)
30. M. Mlejnek, E.M. Wright and J.V. Moloney, Opt.Lett., **23**, 382 (1998)
31. A. Couairon and L.Berge, Phys. Rev. Lett., **88**, 135003 (2002)
32. D. Hollenbeck and C.D. Cantrell, J.Opt. Soc. Am. B, **19**, 2886 (2002)
33. D. Milam, Appl. Opt., **37**, 546 (1998)
34. V.P. Kandidov et al., Appl. Phys. B, **77**, 149 (2003)
35. M. Geissler et al., Phys. Rev. Lett., **83**, 2930 (1999)
36. J.V. Moloney and A.C. Newell, *Nonlinear Optics*, (Perseus Press) (2004).
37. T. Brabec and F. Krauss, Phys. Rev. Lett., **78**, 3282 (1997)
38. A.V. Husakou and J. Herrmann, Phys. Rev. Lett., **87**, 203901 (2001)
39. F. Theberge et al. , Opt. Commun**. 245** 399 (2005)
40. F. Theberge et al., Appl. Phys. B **80** 221 (2005)
41. M. Kolesik et al., Appl. Phys. B submitted (2006)
42. M. Rodriguez et al., Phys. Rev. E, **69** 036607 (2004)
43. K. Stelmaszczyk et al., Appl. Phys. Lett., **85** 3977 (2004)
44. M. Kolesik, E.M. Wright and J.V. Moloney, Phys. Rev. Lett., **92**, 253901 (2004)
45. A. Couairon et al., Phys Rev. E **73** 016608 (2006)
46. M.A. Porras et al. Opt. Lett. **30** 3398 (2005)